PAPER

Check for updates

Bacterial bioluminescence shows nanotexturing does not enhance antibacterial efficacy of zinc oxide membrane coatings

Nicholas Lin, [iD] †‡ [a] Geoffrey McKay, [iD] [b] Dao Nguyen, [iD] [bcd]
Nathalie Tufenkji [iD] *[a] and Christopher Moraes [iD] *[adefg]

Antibacterial membranes are often proposed for applications in which the membranes are in contact with the human body or in contact with food or drink, and hence their designs must minimize unintended toxicity. Zinc oxide (ZnO) is a well-known antibacterial agent and is relatively nontoxic, making it a promising material for the design of antibacterial membranes. Needle-like ZnO nanomaterials are believed to be additionally capable of a cell puncturing mechanism when they are agitated in suspension with bacteria. It is unclear, however, whether the puncturing mechanism is effective when the needle-like nanomaterials are immobilized as surface coatings. In this study, we assessed the antibacterial performance of two types of ZnO coatings synthesized on nylon membranes. One ZnO coating possessed no distinct hierarchical structure whereas the second consisted of ZnO microflowers each comprised of numerous ZnO nanoneedles, collectively forming a nanoneedle topography on the membrane surface. For antibacterial assessment of these coatings, we used several conventional assays and a variation of a recently developed bacterial bioluminescence monitoring assay. The conventional assays evaluated the antibacterial effects of zinc released from the membranes. The bioluminescence monitoring assay uniquely captured antibacterial effects of cell–surface contact between bacteria and the ZnO nanoneedle topography such as the puncture mechanism in question in real time without disturbing ongoing cell–surface interactions throughout incubation. Bioluminescent *Staphylococcus aureus* and bioluminescent *Pseudomonas aeruginosa* exposed to the ZnO nanoneedle topography exhibited loss and recovery of bioluminescence comparable to bacteria that were exposed to the ZnO coating without nanoneedle topography. We conclude that the nanotextured topography therefore did not further enhance antibacterial performance of the ZnO-coated membranes. *S. aureus* and *P. aeruginosa* were able to survive, recover, and proliferate directly atop the nanotextured ZnO coating.

[a] *Department of Chemical Engineering, McGill University, 3610 University Street, Montréal, Québec, H3A 0C5, Canada. E-mail: nathalie.tufenkji@mcgill.ca, chris.moraes@ubc.ca; Tel: +1 514 398 2999, +1 514 398 4278*

[b] *Meakins-Christie Laboratories, Research Institute of the McGill University Health Centre, 1001 Décarie Boulevard, Montréal, Québec, H4A 3J1, Canada*

[c] *Department of Microbiology and Immunology, McGill University, 3775 University Street, Montréal, Québec, H3A 2B4, Canada*

[d] *Department of Medicine, McGill University, 1001 Décarie Boulevard, Montréal, Québec, H4A 3J1, Canada*

[e] *Department of Biomedical Engineering, McGill University, 3775 University Street, Montréal, Québec, H3A 2B4, Canada*

[f] *Rosalind and Morris Goodman Cancer Research Center, McGill University, 1160 Pine Avenue West, Montréal, Québec, H3A 1A3, Canada*

[g] *Division of Experimental Medicine, McGill University, 1001 Décarie Boulevard, Montréal, Québec, H4A 3J1, Canada*

† Current address: School of Architecture and Landscape Architecture, University of British Columbia, 6333 Memorial Road, Vancouver, British Columbia, V6T 1Z2, Canada.

‡ Current address: Department of Microbiology and Immunology, University of British Columbia, 2350 Health Sciences Mall, Vancouver, British Columbia, V6T 1Z3, Canada.

1. Introduction

Antibacterial membranes are often proposed for applications such as potable water filters,[1] absorbent pads in food packaging,[2] and wound dressings.[3] In many of these applications, the membranes are either in direct contact with the human body or in contact with food or drink. Antibacterial agents to be incorporated into the membranes must therefore balance antibacterial efficacy against unintended toxicity.

Zinc oxide (ZnO), a commonly employed antibacterial agent in existing commercial products, is relatively nontoxic to the human body with well-characterized routes of exposure.[4–7] Antibacterial effects of ZnO are greatly augmented at the nanoscale.[5] Antibacterial effects of ZnO nanomaterials were originally attributed to the release of solubilized ionic zinc. Contributions of other mechanisms such as the generation of reactive oxygen species, electrostatic interactions with the bacterial membrane as well as the cellular internalization of

Table 1 Summary of conventional assessment methods for the efficacy of antibacterial material based on classifications by Cunliffe et al.[18]

Assessment methods	General description
High surface area-to-volume ratio assays (e.g. ISO 22196:2011)	A bacterial suspension is pressed between a candidate antibacterial material and an inert surface during incubation, then the bacterial suspension is removed and sampled for viability
Agar zone of inhibition assays (e.g. ISO 20645:2004)	A candidate antibacterial material is placed on a lawn of bacteria growing on an agar plate. After incubation, the size of the zone without visible growth surrounding the antibacterial material is proportional to its antibacterial efficacy
Suspension assays (e.g. ASTM E2149-13a)	A candidate antibacterial material or its leachate is incubated in a liquid medium that is inoculated with bacteria. After a period of incubation, the liquid is sampled to determine bacterial viability
Adhesion assays (e.g. ASTM E3371-22)	A candidate antibacterial material is first exposed to bacteria for a set duration, then an attempt is made to remove adhered bacteria, and then the remaining amount of attached bacteria is quantified
Biofilm assays (e.g. ASTM E2647-20)	A candidate antibacterial material is inoculated with bacteria and incubated in conditions that favor biofilm growth, then presence of biofilm formation is confirmed

ZnO have also gained considerable research attention.[5,8–11] These mechanisms combine to inhibit bacterial uptake of essential cofactors, denature proteins, perturb membrane equilibrium, and interfere with DNA replication and cell division.[5,8–11] More recently, researchers have reported that certain ZnO nanostructures can provide a physical puncture mechanism of action. Cai et al. synthesized three types of microscale ZnO "flowers" in suspension. Each microflower consisted of several nanoscale "petals" radiating from its center.[12] When suspended with bacteria under constant agitation, the authors found sharper petal structures punctured bacterial membranes. Rutherford et al. synthesized needle-like ZnO particles and concluded they were superior to commercial ZnO nanospheres in terms of antibacterial performance.[13] They found agitation provided necessary kinetic energy for the needle-like clusters to contact bacteria with sufficient force to damage bacterial membranes whereas static conditions produced inferior antibacterial performance. The puncture mechanism has also been reported in urchin-like titanium dioxide nanoparticles and nanoparticles with an urchin-like bismuth shell, both under some form of mechanical agitation.[14,15] For consistency in terminology, we refer to these types of structures generally as microflowers since they are similar microscopic particles with hierarchical morphologies of radial nanoscale protrusions. Studies of the antibacterial efficacy of microflowers have mostly focused on their colloidal form in aqueous suspensions under agitation. Whether the puncture mechanism of microflowers is effective when they are immobilized as membrane coatings is unclear because in this use-case the kinetic energy associated with agitation – which appears to be an important criterion for the physical puncture mechanism of sharp nanostructures[13–17] – is notably absent.

To investigate whether the puncture mechanism is appreciable for ZnO microflowers immobilized as nanotextured membrane coatings, we synthesized and compared two types of ZnO coatings onto nylon membranes. One type of coating possessed no distinct hierarchical structure whereas the other coating consisted of ZnO microflowers each comprised of numerous ZnO nanoneedles, thus forming a nanotextured surface. We first performed diffusion-based assays for the antibacterial assessment of the ZnO-coated membranes, including shaking flask incubation, disc diffusion, and growth curves quantified by optical density using the Gram-positive *Staphylococcus aureus* and the Gram-negative *Pseudomonas aeruginosa* as model pathogenic bacteria. However, these conventional assays (summarized in Table 1) provided insights regarding antibacterial efficacy of zinc released from the ZnO-coated membranes but were not designed to assess effects of cell–surface contact between the bacteria and the topography of the coatings.

For the antibacterial assessment of the nanotextured topography specifically, we employed a variation of a recently developed bacterial bioluminescence monitoring assay with bioluminescent strains of *S. aureus* and *P. aeruginosa*.[19–21] In these strains, bioluminescence is a real-time indicator of bacterial metabolic activity (Fig. S1). For example, sudden loss of bioluminescence suggests acute bacterial inactivation, whereas a sustained increase in bioluminescence is indicative of bacterial proliferation.[22–28] In our bioluminescence monitoring assay, we cast agar into wells of a 96-well microplate, placed the ZnO-coated membranes on top of the agar, dispensed a droplet of bioluminescent *S. aureus* or bioluminescent *P. aeruginosa* directly onto the membranes, then monitored bioluminescence intensity over time. This approach ensured cell–surface contact between the bacteria and the membrane coatings was not disturbed while we monitored the resulting real-time loss and recovery of bacterial bioluminescence throughout incubation. Insights gained from this assay have implications for future designs of antibacterial nanotextured membrane coatings while the bioluminescence monitoring assay can be applied to other antibacterial membrane candidates.

2. Materials and methods

2.1 Materials

Luria–Bertani (LB) media powder (molecular genetics grade, cat. #BP1426), agar powder (molecular genetics grade, cat. #BP1423), and white 96-well flat-bottom microplates (cat. #07-200-628) were purchased from Fisher Scientific (Québec, Canada), phosphate buffered saline (PBS, 0.01 M phosphate

© 2026 The Author(s). Published by the Royal Society of Chemistry

RSC Appl. Interfaces, 2026, **3**, 112–124 | 113

buffer, pH 7.4, cat. #P4417), zinc acetate dihydrate (>98%, cat. #383058), hexamethylenetetramine (>99%, cat. #398160), zinc nitrate hexahydrate (98%, cat. #228737), sodium hydroxide (98%, cat. #S5881), cation-adjusted Mueller–Hinton powder (MHBII, cat. #90922), and Whatman® nylon membranes (nominal pore size: 0.2 μm, diameter: 25 mm, cat. #WHA7402002) from Sigma Aldrich (Ontario, Canada), clear 96-well flat-bottom microplates (cat. #229596) from Ultident Scientific (Québec, Canada), and anhydrous ethanol from Commercial Alcohols (Ontario, Canada).

2.2 Preparation of ZnO-coated membranes

ZnO-coated membranes were prepared in three steps adapted from a protocol by Li et al.[29] First, ZnO nanoparticles were synthesized in an ethanol suspension. Next, nylon membranes were seeded in the nanoparticle suspension. Finally, the membranes were placed in a zinc solution to synthesize the ZnO coating hydrothermally.

To synthesize ZnO nanoparticles, a 40 mL solution of 2 mM zinc acetate dihydrate and a 20 mL solution of 4 mM sodium hydroxide were prepared separately in anhydrous ethanol at 80 °C under constant magnetic stirring for 30 min, then cooled in ambient conditions to room temperature. Slowly, the sodium hydroxide solution was poured into the zinc acetate dihydrate solution under magnetic stirring, then the mixture was placed in an oven at 70 °C for 1 h to form ZnO nanoparticles. The Z-average (hydrodynamic size) from dynamic light scattering (Zetasizer NanoZS, Malvern Panalytical Ltd., Worcestershire, United Kingdom) of the synthesized ZnO nanoparticles in ethanol was 87.22 ± 3.74 nm with polydispersity index of 0.252 ± 0.037. Using forceps, nylon membranes were dipped into this nanoparticle suspension then dried in a 70 °C oven for 1 min to seed the membranes with ZnO nanoparticles. This step was repeated two more times to ensure thorough seeding of the membrane. Afterwards, the membranes were placed horizontally in a pre-heated furnace at 120 °C for a total of 30 min (membranes were flipped after the first 15 min such that both sides were subjected to the same treatment) then removed and cooled in ambient conditions to room temperature to remove moisture. Finally, 100 mL of a 25 mM equimolar solution of zinc nitrate hexahydrate and hexamethylenetetramine was prepared in a glass bottle. Seeded membranes were placed vertically in the solution by leaning them against the bottle's inner wall, and the bottle was placed in an oven at 70 °C for 6 h or 12 h. During this time, ZnO crystal growth took place on the surfaces of the seeded membranes.[30–32] Afterwards, membranes were removed and washed three times with DI water and dried at 70 °C overnight, then autoclave-sterilized (121 °C, 15 psi, 10 min) in a glass beaker, at which point the ZnO-coated membranes were ready for analysis.

2.3 Characterization of nylon membranes coated with ZnO microflowers

Membranes with and without ZnO coatings were imaged by scanning electron microscopy (SEM, SU3500, Hitachi Hi-

Technologies, Tokyo, Japan) under variable-pressure mode, which allowed direct observations of the membranes without the need for any additional sample processing or conductive coating steps.

Thermogravimetric analysis (TGA) was performed to verify that membranes with and without ZnO coatings could withstand the temperature of autoclave sterilization (121 °C) necessary prior to any antibacterial assessment. Samples of the membranes (1 to 2 mg) were mounted in open 70 μL alumina crucibles and placed on a TGA/DSC 1 instrument (Mettler Toledo, OH, United States) recording TGA. All experiments were conducted under a stream of nitrogen (25 mL min^{-1}) from room temperature to 600 °C at a rate of 10 °C min^{-1}.

Inductively coupled plasma optical emission spectrometry (ICP-OES, iCAP 6500, Thermo Fisher Scientific, MA, United States) was performed to quantify the amount of zinc released from the membranes. Membranes with and without ZnO coatings were individually placed into 50 mL digitubes (SCP Science, Québec, Canada) each containing 10 mL of DI water. Tubes were wrapped in aluminum foil to minimize light exposure and incubated at 37 °C for 24 h. Next, the membranes were discarded, and contents of the tubes were digested with nitric acid for 4 h at 95 °C for analysis.

2.4 Bacterial cell culture

Bioluminescent S. aureus (generously provided by Plaut et al.[19]) and bioluminescent P. aeruginosa (previously described in Lin et al. and Farkas et al.[20,21]) were genetically engineered to constitutively express the Photorhabdus luminescens lux operon. Frozen (−80 °C) glycerol stock cultures of wildtype S. aureus ATCC 25923, wildtype P. aeruginosa PA01, bioluminescent S. aureus and bioluminescent P. aeruginosa were streaked onto LB agar plates which were then incubated at 37 °C overnight. A single bacterial colony from each plate was looped to inoculate separate 15 mL centrifuge tubes each containing 3 mL of sterile LB broth. The tubes were incubated for ~15 h under orbital shaking (120 rpm, 37 °C) then used to reinoculate 3 mL of fresh LB broth in new centrifuge tubes at a 1:50 ratio for another 2.5 h to reach mid-exponential growth phase (OD ~0.3 for S. aureus cultures and OD ~0.4 for P. aeruginosa cultures), at which point they were harvested to prepare working bacterial suspensions. Unless otherwise stated, the working suspensions were prepared by centrifuging the tubes (Heraeus Multifuge X3R, Thermo Fisher Scientific, MA, United States) at room temperature at 3000 × g for 4 min, decanting the supernatant, then resuspending the pellet in PBS. This step was performed twice. The final bacterial concentration of the working suspension was adjusted with PBS to the desired optical density measured at 600 nm (OD600) using a UV-visible spectrophotometer (BioMate 3S, Thermo Fisher Scientific, MA, United States). The desired OD600 varied depending on the experiment.

2.5 Shaking flask and disc diffusion assays

Shaking flask assays were traditionally performed in Erlenmeyer flasks. Here, the flasks were replaced with pre-sterilized 15 mL

114 | RSC Appl. Interfaces, 2026, 3, 112–124

© 2026 The Author(s). Published by the Royal Society of Chemistry

centrifuge tubes. In each tube, 3 mL of leachate (obtained by immersing the autoclave-sterilized membranes in 10 mL of sterile LB broth in separate ICP-grade digitubes for 24 h) was inoculated with 30 μL of mid-exponential phase wildtype *S. aureus* or wildtype *P. aeruginosa* adjusted to OD600 ~0.1, and then incubated for 24 h under constant orbital shaking (120 rpm, 37 °C). Afterwards, the tubes were sampled, serially diluted, and immediately plated onto LB agar to be incubated overnight at 37 °C for colony counting to quantify the effects of zinc released from the membranes on the viability of bacteria. Colony forming units were reported in log base 10 notation, or $\log_{10}$ (CFU mL^{-1}). Uncoated nylon membranes served as the control in this and all other assays.

For the disc diffusion assay, bacterial lawns were prepared by dispensing 100 μL of mid-exponential phase wildtype *S. aureus* or wildtype *P. aeruginosa* resuspended in PBS to OD600 ~0.3 onto MHBII agar plates, then spreading the bacterial suspensions thoroughly across the agar plates using rolling glass beads for 1 min per plate. Membranes with and without ZnO coatings were hole punched into 6 mm discs using a handheld office hole puncher, autoclave-sterilized (121 °C, 15 psi, 10 min), then placed on the bacterial lawns using forceps. Each plate was divided into two halves (*i.e.*, two technical replicates). Each half supported one disc each of uncoated nylon membrane, and membranes coated with ZnO synthesized for 6 h or 12 h approximately equidistant from one another. Plates were incubated for 24 h, then visually inspected for zones of inhibition around the discs.

2.6 Growth curves

Growth curves were performed by transferring the same leachate-infused LB broth prepared for the shaking flask assay into clear 96-well microplates. Each well contained 150 μL of LB broth with or without leachate. 3 μL of wildtype *S. aureus* or wildtype *P. aeruginosa* at mid-exponential phase and adjusted to OD600 ~0.1 was dispensed into each well. The microplates were incubated under orbital shaking conditions (120 rpm) at 37 °C for 24 h in the microplate reader. OD600 was measured every 30 min. Initial OD600 at t = 0 (OD600$_i$) of each well was used as the blank to subtract the background OD600 value of the LB broth from subsequent OD600 values of the well. All growth curves in this work were performed with the Tecan Spark® multimodal microplate reader (Tecan Group Ltd., Zurich, Switzerland) equipped with active heating and cooling functionality.

The time spent in lag phase before the inflection point which represents onset of exponential growth was defined as the lag time (h). This inflection point was determined *post hoc* with the microbial lag phase duration calculation application developed by Smug *et al.*[33] Input data consisted of OD600 measured every 30 min from t = 0 h to t = 12 h. Calculations were performed with the max growth acceleration method, which identified the time point at which the second derivative of the growth curve is maximal. On average, this onset was determined to be approximately 3 h after inoculation for bioluminescent *S. aureus*

and bioluminescent *P. aeruginosa* in LB media without membranes. Additional details are available the SI (Fig. S1).

2.7 Bioluminescence monitoring assays

All bioluminescence monitoring assays in this work were prepared in white 96-well flat-bottom microplates and performed with the Tecan Spark® with integration time (time allotted for the luminescence detector to collect photons) of 1000 ms per well. Bioluminescence was reported in arbitrary units (AU).

Two types of bioluminescence monitoring assays were developed for this study, a 24 h assay and a 1 h assay. For both types of assays, each well of a white 96-well microplate was first prepared by dispensing 130 μL of molten LB agar, allowing it to cool, then dispensing another 20 μL of molten agar, for a total of 150 μL of agar. This two-step dispensing technique created a flat layer of agar in each well, eliminating the meniscus produced if all 150 μL of agar was dispensed at once. Next, uncoated or ZnO-coated membranes were hole punched into 6 mm discs. The discs were separately placed on top of the agar in wells using forceps. Working suspensions of mid-exponential phase bioluminescent *S. aureus* and bioluminescent *P. aeruginosa* were adjusted to OD$_{600}$ ~0.1 in PBS, then 3 μL of either bacterial suspension was dispensed onto each membrane disc by micropipette. Immediately afterwards, the microplate was lidded then inserted into the microplate reader (pre-heated to 37 °C). Bioluminescence was measured every 30 min for 24 h in the 24 h assay or every 1 min for 60 min in the 1 h assay. For the 24 h assay, lag time (h) of bacterial growth between initial inoculation and onset of exponential phase was defined as the time interval required for bioluminescent *S. aureus* or bioluminescent *P. aeruginosa* to reach 3000 AU or 300 000 AU, respectively. Additional details are available in Fig. S1 and SI text.

2.8 Data visualization and statistical analysis

Graphs were prepared with the Python 3 data visualization packages Matplotlib v3.10.0 and Seaborn v0.13.2 in the Google Colaboratory integrated development environment and statistical analyses were performed with the statistical package JASP v0.16.4. $P < 0.05$ was considered statistically significant. Figure captions provide information regarding statistical treatments and number of replicates for each type of experiment.

3. Results and discussion

3.1 Characterization of ZnO-coated nylon membranes

In this study, we prepared two types of ZnO coatings onto nylon membranes based on well-established hydrothermal synthesis protocols such as that described by Li *et al.*[29] Fig. 1A and B show the surface of the uncoated nylon membrane as observed by SEM. After 6 h of ZnO synthesis, the membrane appeared to be coated with a layer of ZnO which had yet to develop any noteworthy structure (Fig. 1C and D). After another 6 h of synthesis, for a total of 12 h, the ZnO surface appeared thoroughly coated with needle-like structures (Fig. 1E and F)

© 2026 The Author(s). Published by the Royal Society of Chemistry
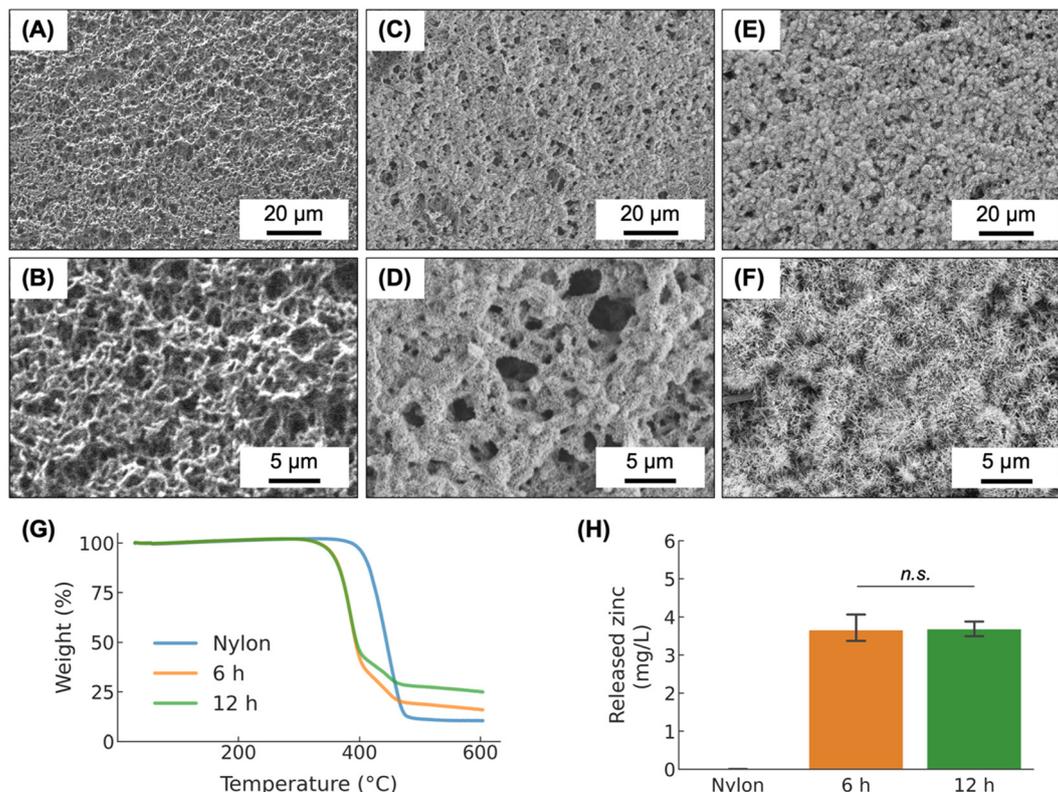
RSC Appl. Interfaces, 2026, **3**, 112–124 | 115

Fig. 1 Low and high magnification SEM images of surface of (A and B) uncoated nylon membrane, (C and D) nylon membrane coated with ZnO after 6 h of synthesis, and (E and F) nylon membrane coated with ZnO after 12 h of synthesis. The ZnO crystals self-assembled into microflowers after 12 h of synthesis. Fig. S2 displays the same images as Fig. 1E and F at a larger format. (G) TGA of membranes showed all types of membranes could withstand temperatures beyond 121 °C. (H) Amount of zinc released from the ZnO-coated membranes after 24 h immersion in DI water was $\sim$3.5 mg L^{-1} (compared to $\sim$0.005 mg L^{-1} detected for uncoated nylon membrane), one-tailed t-test (n = 3), error bars represent standard error.

consistent with that reported by Li *et al.*[29] TGA verified that the uncoated nylon membrane and the two types of ZnO-coated membranes could withstand 121 °C (Fig. 1G). Thus, for all antibacterial assessments in our study, we autoclave-sterilized the membranes at 121 °C for 15 min in preparation for experiments. While the microscopic appearance of membranes coated with ZnO crystals grown for 6 h and 12 h differed considerably, we found no significant difference between the amount of zinc released from the two membranes (Fig. 1H). After 24 h of immersion in water, both types of ZnO-coated membranes released approximately 3.5 mg L^{-1} of zinc, which can be attributed to a combination of ionic zinc and some ZnO crystals that may have detached from the membranes during immersion. Evidently, the microflower architecture did not result in an increased amount of solubilized ionic zinc. Finally, when 3 μL droplets of DI water were dispensed onto the dry membranes, the droplets immediately wicked into the membranes, with or without ZnO coatings, demonstrating that membrane wettability was not noticeably changed after the incorporation of ZnO.

3.2 Shaking flask and disc diffusion assays

We performed several conventional assays to assess antibacterial efficacy of the ZnO-coated membranes. *S. aureus*

and *P. aeruginosa* were chosen as model pathogenic bacteria in this study to represent microorganisms with Gram-positive and Gram-negative cell wall structure, respectively. Cell wall structure is an important consideration in the design of antibacterial materials, as some antibacterial mechanisms are more effective against Gram-positive bacteria whereas others are more effective against Gram-negative bacteria.[34,35] *S. aureus* and *P. aeruginosa* are also members of ESKAPE, a group of six pathogenic bacterial species notorious for their antibiotic resistance and often associated with hospital-acquired infections.[36,37]

We performed several conventional assays to assess antibacterial performance of the ZnO-coated membranes. In an experiment to evaluate the antibacterial effects of zinc released from the ZnO-coated membranes, we collected leachate from the membranes by immersing the sterilized membranes in LB broth for 24 h. This broth, now infused with released zinc from the ZnO-coated membranes, was transferred to centrifuge tubes, inoculated with *S. aureus* or *P. aeruginosa*, incubated for 24 h under constant orbital shaking, then sampled for cell enumeration.

We found no difference in viable colony counts (Fig. 2) between the two types of ZnO-coated membranes. This was to be expected since the amounts of zinc released from both ZnO-coated membranes were approximately the same ($\sim$3.5
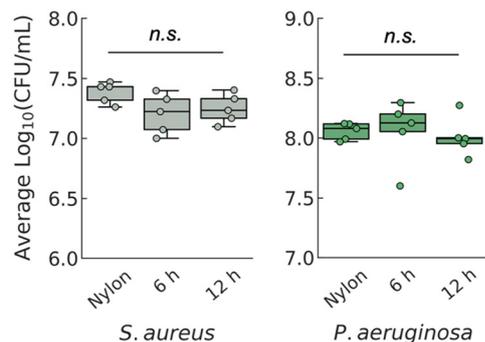
Fig. 2 Colony counting for cell enumeration of *S. aureus* and *P. aeruginosa* found no significant loss of cell population when exposed to leachates from ZnO-coated membranes, ANOVA (*n* = 5).
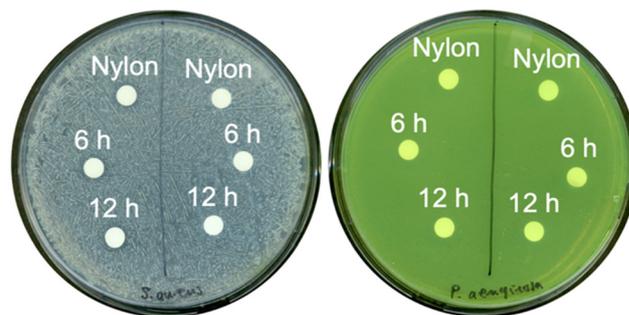

Fig. 3 Disc diffusion yielded no clear zones of inhibition after 24 h for *S. aureus* (left) or *P. aeruginosa* (right) plates. The assay was performed with 3 separate MBHII plates (*n* = 3) for each species. Each plate consisted of 2 technical replicates.

mg L^{-1} each, Fig. 1H). Furthermore, exposure to leachate from the ZnO-coated membranes did not reduce the number of viable bacteria. This was also unsurprising, since zinc's reported minimal inhibitory concentration is typically several orders of magnitude higher, on the order of 10–100 mg L^{-1}, than what was present in the leachates.[38,39]

The disc diffusion assay produced similar results. In this assay, discs are usually imbued with a candidate antibacterial agent before being placed on a lawn of bacteria grown on agar plates. During incubation of the plates, the agent diffuses out of the discs, and clear zones free of visible growth, referred to as zones of inhibition, form around the discs if the antibacterial agent is indeed effective at the prepared concentration. In our study, the discs were our nylon membranes already coated with ZnO as the intended antibacterial agent thus they were used as-is to evaluate the antibacterial efficacy of zinc released from the membranes. We found both types of ZnO-coated membranes showed no clear zones of inhibition on *S. aureus* and *P. aeruginosa* plates after 24 h of incubation (Fig. 3).

3.3 Growth curves

Both shaking flask and disc diffusion assays showed that the amount of released zinc yielded no antibacterial effects by the end of the incubation period. To assess whether the released zinc possessed any initial inhibitory effects at the beginning of the incubation period, we transferred the same leachate-infused LB broth from the shaking flask assay into 96-well microplates, inoculated the wells with *S. aureus* or *P. aeruginosa*, then monitored real-time growth of bacteria throughout a 24 h period by optical density.

S. aureus exposed to leachate from uncoated nylon reached exponential phase growth after mean lag time of ~3.5 h (Fig. 4A). The presence of zinc released from the ZnO-coated membranes inhibited the onset of exponential growth by an additional ~2 h, for a total lag time of ~5.5 h. *P. aeruginosa* exposed to leachate from uncoated nylon reached exponential phase growth after mean lag time of ~3 h and the presence of zinc leachate inhibited exponential growth by another ~2.5 h (Fig. 4B). Other than the shifted lag times, no

other aspects of the zinc leachate growth curves appeared visually different from their respective controls (leachate from uncoated nylon membrane). After 24 h of incubation in LB broth, both *S. aureus* and *P. aeruginosa* exposed to zinc leachate fully recovered to levels comparable to their respective controls. This confirmed that the released zinc inhibited growth initially, but bacteria were still viable, which explained our results from the shaking flask and disc diffusion assays. Furthermore, we found no statistical difference in antibacterial performance between the leachates prepared from membranes coated with ZnO crystals grown for 6 h and 12 h (Fig. 4C), which was expected since they leached the same amount of zinc (Fig. 1H). Based on these assays, we can conclude that the microflower coating did not provide any enhanced antibacterial effects attributable to released zinc.

3.4 Design of bioluminescence monitoring assay

Most conventional antibacterial assessment techniques operate on the assumption that the material is releasing an antibacterial agent into the environment, and it is this released agent that is responsible for antibacterial activity.[40] For example, the previous assays (Fig. 2–4) provided information regarding antibacterial effects of zinc released from the ZnO-coated membranes. These assays could not detect potential effects of cell–surface contact between the bacteria and the membrane coatings. In a preliminary experiment to evaluate these effects, we incubated bacteria directly onto nanotextured membranes (Fig. S3). We observed visible colony growth on the membranes after incubation thus concluded that even direct cell–surface contact with highly textured ZnO was not bactericidal. Whether cell–surface contact produced initial inhibitory effects was unclear as this experiment also lacked real-time sensitivity. Therefore, we designed an assessment method that miniaturized this contact-based assay, enabling us to monitor real-time bacterial bioluminescence in a 96-well microplate format to detect for initial inhibitory effects of cell–surface contact.
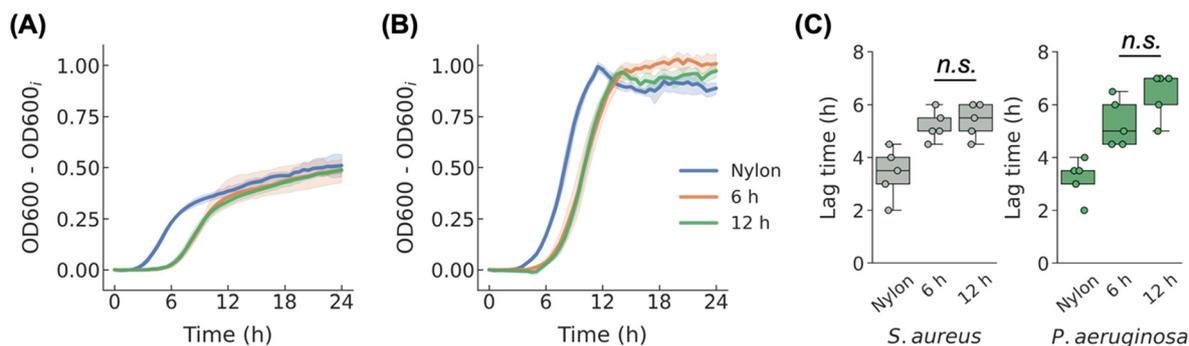
© 2026 The Author(s). Published by the Royal Society of Chemistry

RSC Appl. Interfaces, 2026, **3**, 112–124 | 117

Fig. 4 Average absorbance (OD600) of (A) wildtype *S. aureus* or (B) wildtype *P. aeruginosa* grown in LB infused with leachate from nylon membranes (n = 5) monitored over 24 h (measured every 30 min), shadings represent 95% confidence intervals. (C) Lag time before exponential bacterial growth as a result of exposure to leachates, ANOVA, Bonferroni *post hoc* (n = 5). Full statistical comparisons are available in Table S1.

In this assay, 150 μL of molten LB agar was first cast into each well, then allowed to cool to room temperature. An uncoated nylon membrane disc or ZnO-coated membrane disc was then placed on top of the layer of agar within each well (Fig. 5A). Next, a droplet of bioluminescent bacteria was dispensed onto each membrane disc by micropipette, after which the microplate was monitored for real-time changes in bioluminescence over time *via* the luminescence detector of a microplate reader. This bioluminescence monitoring assay uniquely combined four advantages. First, cell–surface contact was consistently maintained and undisturbed throughout incubation, even as real-time measurements were recorded and nutrients were supplied *via* the LB agar. Second, the membranes and bacteria were wetted by the agar throughout incubation, eliminating confounding effects of desiccation. Third, the design better reflects applications in which a membrane is subjected to nutrient-rich conditions but not submerged in liquid, such as wound exudates in wound dressing applications or meat exudates in meat packaging applications. Fourth, the design leveraged the high-throughput capacity and speed of the microplate reader so that as many as 96 membrane samples could be monitored simultaneously.

In designing the bioluminescence monitoring assay, we found bioluminescence intensity detected at the peak of *P. aeruginosa* exponential growth was not correlated to volume of the agar in the well (Fig. 5B and S4). We deposited 150 μL of agar per well because this volume resulted in consistently high detectable bioluminescence and was more straightforward for experimental preparations. Additional details are provided in the SI text. Contents in a microplate experiment are typically liquid, whereas we have adapted the microplate for the assessment of antibacterial membrane discs. To verify that bleed-through of bioluminescence signal from one well to the next was minimal in our design, we first dispensed a concentrated (OD600 ~1) droplet (3 μL) of mid-exponential phase bioluminescent *P. aeruginosa* into a central well (position 0 in Fig. 5C) as a source of bioluminescence signal, then measured the bioluminescence intensity of its adjacent 5 wells with the microplate lid on. We found average

bleed-through from position 0 to its immediately adjacent wells (position −1 and position 1 in Fig. 5D) was less than 0.2%, which we deemed negligible given that we were interested in bioluminescence changes over orders of magnitude. Thus, all 96 wells of the microplate were available for experiments, if necessary.

In selecting the bacterial concentration in the droplet, we found bacterial bioluminescence was linearly proportional with respect to bacterial concentration (OD600 adjusted in PBS) immediately after they were deposited on the membranes (Fig. 5E and F). Since the working suspensions for our previous growth curves were prepared at OD600 ~0.1 at mid-exponential phase, this concentration and phase of growth were also used for the bioluminescence monitoring assays for consistency. For reference, at this concentration, average bioluminescence of *S. aureus* and *P. aeruginosa* was 2103 AU and 11 227 AU, respectively. We deposited 3 μL droplets of bioluminescent *S. aureus* or bioluminescent *P. aeruginosa* adjusted to OD600 ~0.1 on the membrane discs on top of the agar, then immediately monitored real-time change in bioluminescence in a microplate reader maintained at 37 °C. We used the metric of lag time before onset of exponential growth to compare potential bacterial inhibition.

3.5 24 h and 1 h bioluminescence monitoring

In the 24 h bioluminescence monitoring assay, we noticed the shape of the bioluminescence curve over time for *S. aureus* deposited on uncoated nylon membranes (Fig. 6A) exhibited comparable qualities to that of bioluminescent *S. aureus* grown in aqueous media without membranes (Fig. S1C). This was not surprising, as proteomics have found cells grown on agar are physiologically similar to free-floating cells growing in aqueous media.[41] In contrast, growth of *S. aureus* deposited on the ZnO-coated membranes was inhibited initially but exponential phase was observed in all replicates. *S. aureus* deposited on membranes coated with ZnO synthesized for 6 h and 12 h appeared to recover and proliferate at the same rate. Growth of *P. aeruginosa* deposited on the two ZnO-coated membranes was also initially inhibited but similarly recovered after an extended
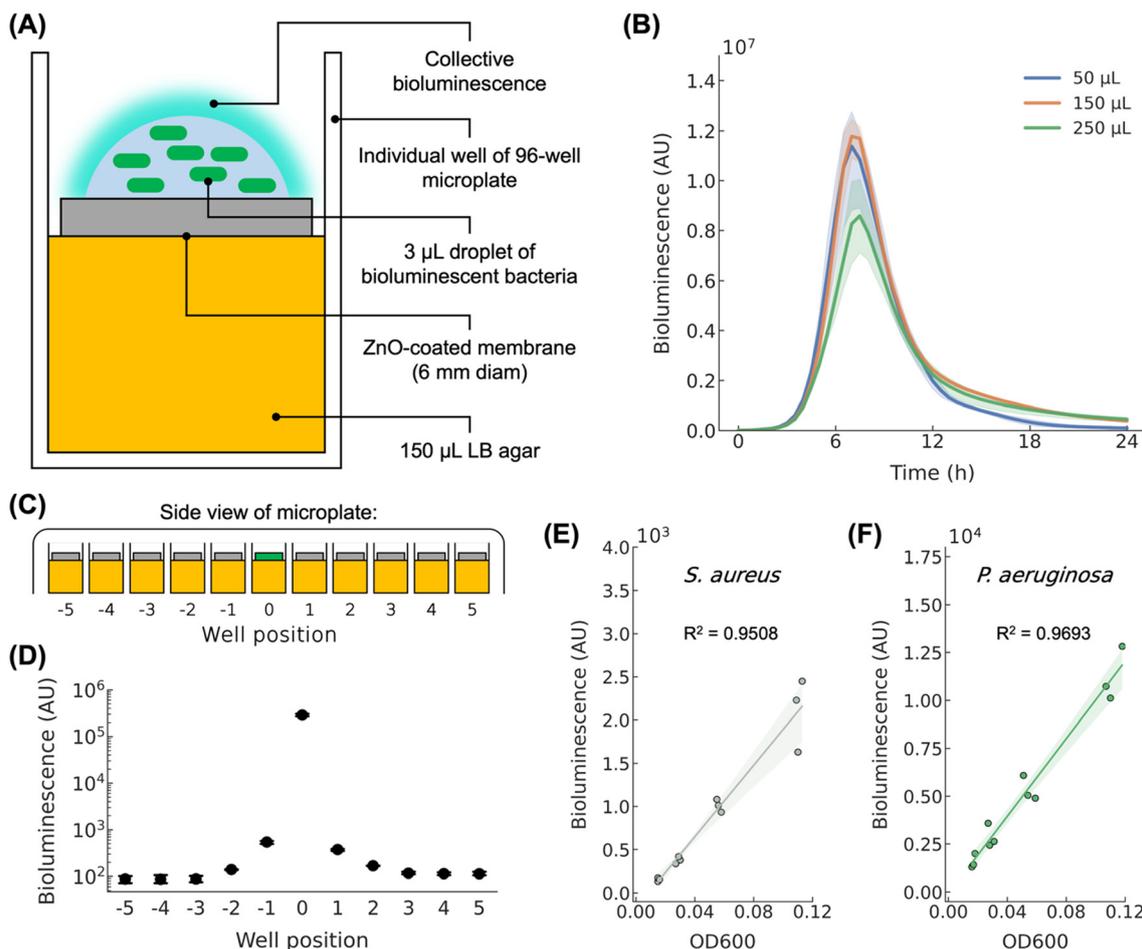
Fig. 5 (A) Schematic of individual well of a white flat-bottom 96-well microplate immediately after deposition of droplet containing bioluminescent bacteria. (B) Average bioluminescence detected from *P. aeruginosa* on membranes on different volumes of LB agar (50 μL, 150 μL, or 250 μL) over 24 h (*n* = 4), shadings represent 95% confidence intervals. (C) Schematic (side view) of microplate with lid on. A concentrated droplet of mid-exponential phase bioluminescent *P. aeruginosa* was dispensed in position 0 as a source of bioluminescence signal. (D) Average bioluminescence at position 0, −1, and 1 were 288 353 AU, 543 AU, and 375 AU, respectively (*n* = 3). Bleed-through experiments for additional configurations, including empty microplate with no bioluminescence source, microplate containing only agar, and microplate without lid, are provided in Fig. S4. (E) Bioluminescence (AU) of *S. aureus* prepared at various concentrations (OD600) immediately after deposition on membrane, shading represent 95% confidence interval. (F) Bioluminescence (AU) of *P. aeruginosa* prepared at various concentrations (OD600) immediately after deposition on membrane, shading represent 95% confidence interval. Schematics are not drawn to scale.

lag phase (Fig. 6B). These results corroborated our observation that bacteria were capable of proliferating directly on the ZnO-coated membranes in a biofilm-like manner after 24 h of incubation (Fig. S3).

Lag times before exponential growth of *S. aureus* and *P. aeruginosa* due to antibacterial effects of cell–surface contact with the ZnO-coated membranes were ~12 h and ~7.5 h respectively (Fig. 6C). Contact with ZnO-coated membranes extended the lag times of *S. aureus* and *P. aeruginosa* by ~8 h and ~4 h, respectively, compared to contact with uncoated nylon membranes. For reference, this shift was approximately 4× and 1.5× the shift in lag times attributed to exposure to leachate alone (~2 h for *S. aureus* and ~2.5 h for *P. aeruginosa*, Fig. 4C). The extended lag times observed in the 24 h bioluminescence assay could be due to several antibacterial mechanisms at the cell–surface interface which are absent or not as effective in the leachate assay. For example, at the

membrane surface, zinc released from the membranes and reactive oxygen species such as peroxides, superoxides, and hydroxyl radicals are likely more concentrated whereas in the leachate they become diluted. Furthermore, these mechanisms may enhance each other, producing synergistic inhibitory effects at the membrane surface that are greater than their independent contributions. Nonetheless, the cell puncture mechanism of the microflowers appeared to be insignificant based on this assay, since the lag times of bacteria incubated on membranes coated with ZnO microflowers were no different from membranes coated with ZnO without hierarchical structures.

Still, initial lag in *S. aureus* and *P. aeruginosa* growth due to contact with ZnO-coated membranes was significant. To better observe these acute effects, we employed the same bioluminescence monitoring assay design (Fig. 6A) but monitored minute-by-minute change in bioluminescence for 1
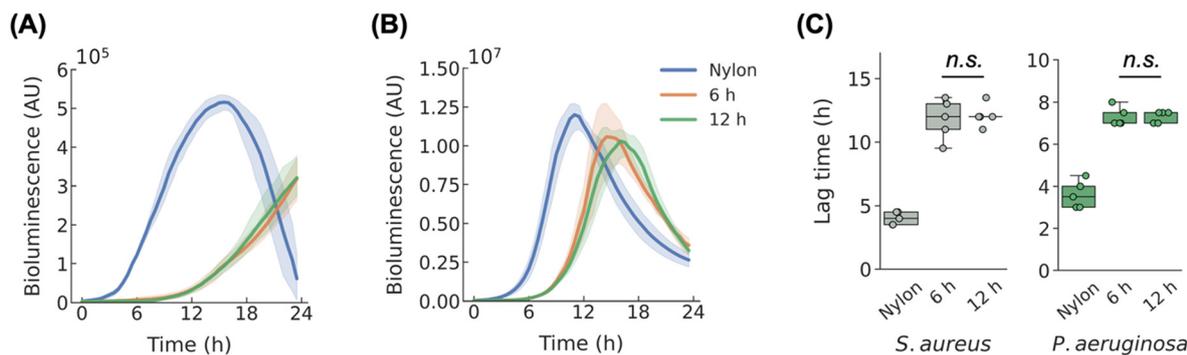
© 2026 The Author(s). Published by the Royal Society of Chemistry

RSC Appl. Interfaces, 2026, **3**, 112–124 | **119**

Fig. 6 Average bioluminescence (AU) from (A) *S. aureus* and (B) *P. aeruginosa* throughout 24 h of membrane contact (measured every 30 min, *n* = 5), shadings represent 95% confidence intervals. (C) Lag time before exponential bacterial growth as a result of cell–surface contact with membranes, ANOVA, Bonferroni *post hoc* (*n* = 5). Full statistical comparisons are available in Table S1.

h immediately upon cell–surface contact. For *S. aureus*, we noticed a slight uptick in bioluminescence across all replicates in the first ~10 min after deposition (Fig. 7A). This was followed by a continued decrease in bioluminescence. For *P. aeruginosa*, we also observed an increase in bioluminescence after deposition (Fig. 7B), but this increase was noticeably more gradual than what we observed in *S. aureus*. We speculate that the initial increase in bioluminescence for both species was triggered in response to the bacteria in the working suspension adjusting to the new nutrient rich environment upon deposition, namely the LB agar surface. At the 1 h mark (Fig. 7C), we found average bioluminescence of *S. aureus* and *P. aeruginosa* deposited on the ZnO-coated membrane discs were significantly lower than on uncoated nylon membrane discs. This suggested that metabolic activity was inhibited as a result of exposure to ZnO-coated membranes, though the underlying mechanism(s) responsible for this inhibition was not clear. Nevertheless, we again found the topography associated with the ZnO microflowers did not enhance antibacterial effects.

Findings of both bioluminescence monitoring assays form a more comprehensive antibacterial assessment: upon contact of *S. aureus* or *P. aeruginosa* cells with ZnO-coated membranes, the cells experienced antibacterial effects which were detectable within the first 60 min of contact. These effects

inhibited onset of exponential growth considerably but were not bactericidal. Eventually, *S. aureus* or *P. aeruginosa* recovered and were able to proliferate again by the 24 h mark, consistent with our conclusions from conventional assays. By definition, bacteriostatic agents inhibit bacterial proliferation but are not capable of rendering cells non-viable.[42] Both types of ZnO-coated membranes in this study exhibited antibacterial effects that were consistent with this definition of bacteriostatic materials but fell short of the definition of bactericidal materials. These findings indicate that long-term antibacterial efficacy is negligible and that biofilm formation would likely occur on the membranes given sufficient time and nutrients.

A leading theory explaining bacterial proliferation on antibacterial surfaces is that cells which deposit and contact the surface are indeed rendered non-viable, but their biomass and extracellular debris act as a barrier between the surface and subsequent cells that deposit shortly after. The newly deposited cells therefore experience sublethal antibacterial effects or are completely unaffected, allowing them to proliferate on the antibacterial surface. This behavior has been observed for many types of antibacterial surfaces and was recently demonstrated by Huang *et al.* for nanotextured surfaces and could also explain our findings.[43]
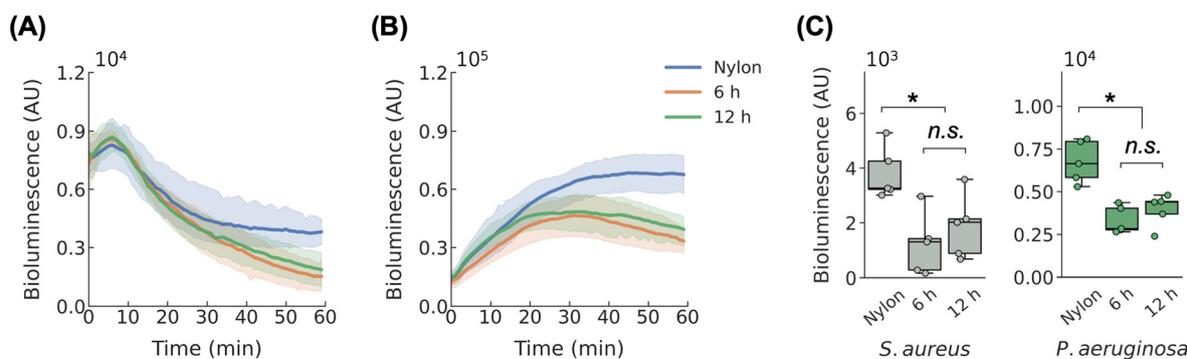

Fig. 7 Average bioluminescence (AU) of (A) *S. aureus* and (B) *P. aeruginosa* throughout 60 min of membrane contact (measured every 1 min, *n* = 5), shadings represent 95% confidence intervals. (C) Bioluminescence after 60 min of cell–surface contact with membranes, ANOVA, Bonferroni *post hoc* (*n* = 5). Full statistical comparisons are available in Table S1.

Table 2 Summary of other studies of porous membranes that incorporated ZnO as the antibacterial agent

Membrane composition	Assessment	Assessment results	Ref.
Composites of ZnO nanoparticles and porous anodic alumina	Adhesion assay, biofilm assay	Generally inhibited growth of *Shewanella putrefaciens* biofilm but did not prevent growth completely	Xu *et al.*[44]
Composites of ZnO nanoparticles and porous polyamide	High surface area-to-volume ratio assay	Highly bactericidal to moderately antibacterial against *S. aureus*, depending on variations in composite formulation	Tang *et al.*[45]
Composites of ZnO nanoparticles, hydroxypropyl methylcellulose, and carboxymethyl starch	Agar zone of inhibition assay	Somewhat inhibited *S. aureus*, weakly inhibited *E. coli*. Higher concentration of ZnO nanoparticles increased antibacterial efficacy	Pitpisutkul *et al.*[46]
Composites of ZnO nanoparticles, reduced graphene oxide (rGO), and polyvinylidene fluoride (PVDF)	Agar zone of inhibition assay	ZnO-PVDF and rGO/ZnO-PVDF showed relatively weak zone of inhibition against *Bacillus subtilis*	Agrawal *et al.*[47]
Composite of ZnO nanoparticles and maize-stalk carbohydrate	Filtration-based assay	Filters trapped and eliminated *E. coli* and *S. aureus*	Gao *et al.*[48]

An examination of other studies of membranes which incorporated ZnO as antibacterial agents shows that our findings are generally consistent with the literature (Table 2).[44–48] Namely, ZnO exhibits moderate antibacterial activity but is not highly potent on its own, though increasing the amount of ZnO in the membrane formulation generally improved antibacterial efficacy.[44–46] This outlines a possible approach to enhance efficacy of ZnO-coated membranes described in this study, namely by increasing the ZnO coating thickness at the membrane surface.

Finally, this assay can be adapted in various ways. For example, the LB agar can be replaced with agar that contains diluted nutrients or substituted with defined media to assess antibacterial efficacy and metabolic recovery in absence of a nutrient-rich environment. This would be particularly relevant if the assay was intended to mimic conditions typically associated with low nutrient availability.[49] Alternatively, the same experimental design can be applied to a candidate antibacterial material is a solid material instead of a membrane, though in this variation the LB agar would not be able to maintain wettability and nutrients so only shorter experiments would be suitable. Furthermore, if either sample size and/or droplet size is to be increased, the experiment could be adapted for different microplate formats (such as 24-well or 6-well) with ease.

3.6 Study limitations

Numerous antibacterial studies have been conducted for ZnO micro- and nanostructures synthesized *via* the hydrothermal route. Colloidal suspensions such as ZnO nanoparticles, ZnO microspheres (Fig. 8A), ZnO microflowers (Fig. 8B), and ZnO nanorods are relatively well-studied while ZnO topographies such as nanoneedles (Fig. 8C) and nanopillars (Fig. 8D) and nanowires have been investigated to a lesser extent.[5–7] In some studies, ZnO materials exhibited exceptional bactericidal effects when coupled with UV illumination, generating reactive oxygen species due to ZnO's photocatalytic properties that damage bacterial membranes and biomolecules.[50,51] Since our objective focused on the speculated puncture effect of the nanotextured membrane surface, experiments were conducted without UV activation and reactive oxygen species were likely minimized. Accordingly, instead of the puncture mechanism, future work could investigate whether ZnO nanotextures produce higher levels of antibacterial reactive oxygen species compared to non-textured ZnO.

Moreover, like many previous ZnO studies, this work employed conventional antibacterial assays (summarized in Table 1), complemented by a bioluminescence monitoring assay for real-time assessment. These assays serve as laboratory screens to select for materials with promising antibacterial performance. However, they offer limited insight in identifying the dominant antibacterial mechanism(s) at play. In general, ZnO nanomaterials offer a combination of antibacterial mechanisms, which we have summarized in the Introduction. Since ZnO nanotexturing failed to enhance antibacterial performance in comparison to the ZnO coating without nanotexturing, we felt conducting a deeper mechanistic analysis (which would include quantifying oxidative stress) was thus outside the scope of this work.

Physical antibacterial mechanisms such as puncture have attracted considerable interest in the search for future antibacterial agents. Highly effective physical mechanisms are expected to reduce our reliance on chemical antibacterial agents, which in turn reduces opportunities for development of antibiotic resistance and minimizes toxicity associated with leached compounds.[35,52] Some studies have observed the puncture mechanism when microflowers were suspended with bacteria in agitated aqueous media. However, we found the immobilized ZnO microflowers as nanotextured membrane coatings offered no appreciable enhancements to antibacterial performance based on conditions assessed. While some cells may have experienced physical puncture mechanism in the manner others have described,[12,13] evidently this mechanism was not the dominant contributor to the antibacterial capabilities we observed with the membranes coated with nanotextured ZnO. We suspect this discrepancy may be attributed to forces necessary to invoke the puncture mechanism which are absent when the microflowers are immobilized. In the literature, kinetic energy associated with agitating, mixing and stirring appears to be an important criterion for the physical puncture mechanism of sharp
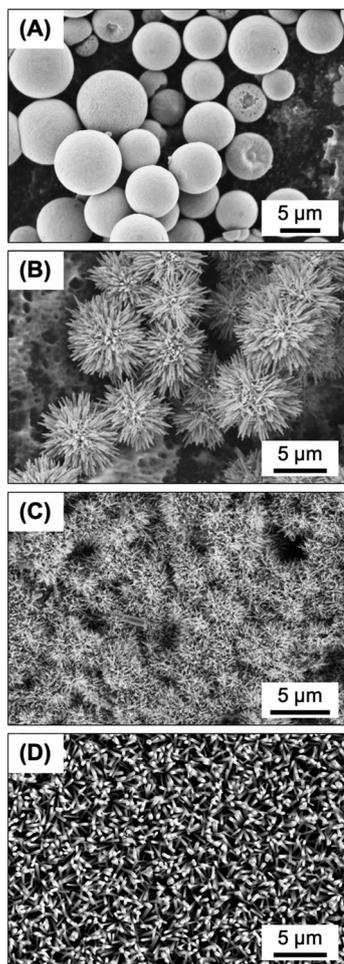
Fig. 8 Plan view SEM images of (A) colloidal ZnO microspheres deposited on carbon tape, (B) colloidal ZnO microflowers deposited on carbon tape, (C) ZnO nanoneedles coated on nylon membrane surface, (D) ZnO nanopillars coated onto glass surface, all prepared *via* hydrothermal synthesis methods.

nanostructures in suspension with bacteria.[13–17] Other works have shown that mechano-bactericidal nanotopographies such as high aspect ratio nanopillars (Fig. 8D) require the application of a normal force to induce acute bacterial cell puncture.[53–56] Therefore, it may be premature to conclude that the nanotextured ZnO coating synthesized in this work would produce no puncture effect in all circumstances. Whereas this study was limited to static *in vitro* assays, more customized assays that introduce shear stress under fluid flow or applied pressure or other forms of external force could be necessary to trigger the puncture mechanism.

Another limitation of this study is that only a single nanoneedle geometry was examined. Other geometries may yield different results. For example, height, diameter, spacing, sharpness, and orientation of topographical nanostructures are parameters that researchers have adjusted while attempting to achieve or enhance the antibacterial performance of nanostructures with varying degrees of success. Diameter of nanostructures and spacing between neighboring nanostructures

appear to be particularly critical, but there exist conflicting recommendations from both theoretical and experimental studies on whether increasing or decreasing these parameters lead to improved antibacterial efficacy.[57–60]

Antibacterial membranes are potentially useful in many applications. The standardized assays summarized in Table 1 as well as the bioluminescence monitoring assay developed for this study serve only as general initial laboratory screens for candidate antibacterial materials. For promising candidate materials, each targeted application requires additional evaluation. For example, the membranes could be used as single-use and point-of-use filters to treat water intended for general-purpose cleaning and sanitation activities, such as showering, laundering, and dishwashing. In this application, degradation and loss of the ZnO coating under prolonged exposure to water would be important to characterize.[61,62] As another example, for nanotextured ZnO membranes intended as food packaging materials, membranes with promising antibacterial properties would be further assessed for potential migration of ZnO or zinc ions from the membrane into food products, ability to prevent biofilm formation, as well as long-term stability over multiple days and in varying levels of pH and salinity. Such evaluations ensure the effectiveness and safety of the material under realistic use conditions and compliance with regulatory standards for food contact materials.[63,64] As another example, for nanotextured ZnO membranes intended as wound dressing materials, additional biocompatibility and cytotoxicity evaluations must be considered to better understand possible side effects when in contact with the human body. These evaluations would include the tetrazolium colorimetric assays (MTT/MTS/XTT) and *in vivo* studies.[65,66]

Collectively, the assays throughout this study conclude that both types of ZnO-coated membranes inhibited initial growth of bacteria. Antibacterial effects of the ZnO-coated membranes were detected within 1 h of cell–surface contact between the bacteria and the membranes. However, given sufficient time and nutrients, bacteria eventually overcame initial inhibition to proliferate again. By definition, bacteriostatic agents delay or inhibit bacterial proliferation, whereas bactericidal agents render bacteria non-viable.[52] Both types of ZnO-coated membranes in this study exhibited antibacterial effects that were consistent with this definition of bacteriostatic agents but fell short of the definition of bactericidal agents. In its current form, we envision the bacteriostatic and nontoxic properties of the ZnO-coated membranes could be safely adapted for applications in which some level of treatment is desirable, but the eradication of bacteria is not required.

4. Conclusions

In this study, we assessed the antibacterial performance of nylon membranes coated with two types of ZnO coatings. One type of coating possessed no distinct hierarchical structure whereas the other coating consisted of ZnO microflowers each comprised of numerous ZnO nanoneedles,

thus forming a nanotextured surface. Using *S. aureus* and *P. aeruginosa* as model pathogenic bacteria, we employed conventional antibacterial assays as well as a bacterial bioluminescence monitoring assay that enabled cell–surface contact between the bacteria and the membrane coating during antibacterial assessment. We found the coating of ZnO microflowers were no more effective compared to the coating of ZnO without distinguishable hierarchical structure under the conditions we evaluated. Both types of coatings possessed acute inhibitory capabilities, but *S. aureus* and *P. aeruginosa* deposited onto the coatings were able to survive, recover, and proliferate directly atop the microflowers.

Conflicts of interest

The authors declare no competing conflicts of interest.

Data availability

Data for this article, including excel files and captured raw images are available *via* the Open Science Framework repository at https://doi.org/10.17605/OSF.IO/Y7CRW.

Supplementary information (SI): supplementary text for the design of the bioluminescence monitoring assays; growth curves and bioluminescence of wildtype and bioluminescent *S. aureus* and *P. aeruginosa* (Fig. S1); larger format of Fig. 1E and F (Fig. S2); visible colony growth on membranes coated with nanotextured ZnO (Fig. S3); bleed-through experiments for various configurations of the 96-well microplate (Fig. S4); schematics representing different microplate measurement modes (Fig. S5); statistical treatment for Fig. 4C, Fig. 6C and Fig. 7C (Table S1); summary table of different microplate measurement modes (Table S2). See DOI: https://doi.org/10.1039/d5lf00048c.

Acknowledgements

References

1 M. Mukherjee and S. De, *Environ. Sci.*, 2018, **4**, 1078–1104.

2 S. Smaoui, I. Chérif, H. Ben Hlima, M. U. Khan, M. Rebezov, M. Thiruvengadam, T. Sarkar, M. A. Shariati and J. M. Lorenzo, *Food Packag. Shelf Life*, 2023, **36**, 101045.

3 D. Simões, S. P. Miguel, M. P. Ribeiro, P. Coutinho, A. G. Mendonça and I. J. Correia, *Eur. J. Pharm. Biopharm.*, 2018, **127**, 130–141.

4 W. Maret and H. H. Sandstead, *J. Trace Elem. Med. Biol.*, 2006, **20**, 3–18.

5 A. Sirelkhatim, S. Mahmud, A. Seeni, N. H. M. Kaus, L. C. Ann, S. K. M. Bakhori, H. Hasan and D. Mohamad, *Nano-Micro Lett.*, 2015, **7**, 219–242.

6 J. Fujihara and N. Nishimoto, *Biol. Trace Elem. Res.*, 2024, **202**, 9–23.

7 V. Nagar, T. Singh, Y. Tiwari, V. Aseri, P. P. Pandit, R. L. Chopade, K. Pandey, P. Lodha and G. Awasthi, *Mater. Today: Proc.*, 2022, **69**, 56–63.

8 H. Moradpoor, M. Safaei, H. R. Mozaffari, R. Sharifi, M. M. Imani, A. Golshah and N. Bashardoust, *RSC Adv.*, 2021, **11**, 21189–21206.

9 B. Abebe, E. A. Zereffa, A. Tadesse and H. C. A. Murthy, *Nanoscale Res. Lett.*, 2020, **15**, 190.

10 E. Albalghiti, L. M. Stabryla, L. M. Gilbertson and J. B. Zimmerman, *Environ. Sci.: Nano*, 2021, **8**, 37–66.

11 R. Kumar, A. Umar, G. Kumar and H. S. Nalwa, *Ceram. Int.*, 2017, **43**, 3940–3961.

12 Q. Cai, Y. Gao, T. Gao, S. Lan, O. Simalou, X. Zhou, Y. Zhang, C. Harnoode, G. Gao and A. Dong, *ACS Appl. Mater. Interfaces*, 2016, **8**, 10109–10120.

13 D. Rutherford, J. Jíra, K. Kolářová, I. Matolínová, J. Mičová, Z. Remeš and B. Rezek, *Int. J. Nanomed.*, 2021, **16**, 3541–3554.

14 Y. Xu, X. Liu, Y. Zheng, C. Li, K. W. Kwok Yeung, Z. Cui, Y. Liang, Z. Li, S. Zhu and S. Wu, *Bioact. Mater.*, 2021, **6**, 1575–1587.

15 Y. Xu, B. Chen, L. Xu, G. Zhang, L. Cao, N. Liu, W. Wang, H. Qian and M. Shao, *ACS Appl. Mater. Interfaces*, 2024, **16**, 3215–3231.

16 K. Matuła, Ł. Richter, W. Adamkiewicz, B. Åkerström, J. Paczesny and R. Hołyst, *Soft Matter*, 2016, **12**, 4162–4169.

17 S. Liu, L. Wei, L. Hao, N. Fang, M. W. Chang, R. Xu, Y. Yang and Y. Chen, *ACS Nano*, 2009, **3**, 3891–3902.

18 A. J. Cunliffe, P. D. Askew, I. Stephan, G. Iredale, P. Cosemans, L. M. Simmons, J. Verran and J. Redfern, *Antibiotics*, 2021, **10**, 1069.

19 R. D. Plaut, C. P. Mocca, R. Prabhakara, T. J. Merkel and S. Stibitz, *PLoS One*, 2013, **8**, e59232.

20 N. Lin, G. McKay, D. Nguyen, C. Moraes and N. Tufenkji, *ACS Appl. Nano Mater.*, 2023, **6**, 18454–18465.

21 E. Farkas, G. A. McKay, L. T. Hu, M. Nekouei, P. Ho, W. Moreira, C. C. Chan, L. C. Dam, K. Auclair, S. Gruenheid, L. Whyte, P. Dedon and D. Nguyen, *Sci. Rep.*, 2024, **14**, 31039.

22 G. Duffy, A. Ellison, W. Anderson, M. B. Cole and G. S. Stewart, *Appl. Environ. Microbiol.*, 1995, **61**, 3463–3465.

23 C. E. R. Dodd, R. L. Sharman, S. F. Bloomfield, I. R. Booth and G. S. A. B. Stewart, *Trends Food Sci. Technol.*, 1997, **8**, 238–241.

24 A. Ellison, S. F. Perry and G. S. A. B. Stewart, *Int. J. Food Microbiol.*, 1991, **12**, 323–332.

© 2026 The Author(s). Published by the Royal Society of Chemistry

RSC Appl. Interfaces, 2026, **3**, 112–124 | 123

25 L. M. Hudson, J. Chen, A. R. Hill and M. W. Griffiths, *J. Food Prot.*, 1997, **60**, 891–897.

26 W. Sun, L. Brovko and M. Griffiths, *J. Ind. Microbiol. Biotechnol.*, 2001, **27**, 126–128.

27 J. Chen and M. W. Griffiths, *Int. J. Food Microbiol.*, 1996, **31**, 27–43.

28 L. Y. Brovko and M. W. Griffiths, *Bioluminescence Lights the Way to Food Safety*, SPIE, 2003.

29 X. Li, Y.-H. Wang, C. Zhao and X. Liu, *ACS Appl. Mater. Interfaces*, 2014, **6**, 22004–22012.

30 S. D. G. Ram, G. Ravi, A. Athimoolam, T. Mahalingam and M. A. Kulandainathan, *Appl. Phys. A: Mater. Sci. Process.*, 2011, **105**, 881–890.

31 P. Ramos, L. Sánchez and J. Rodríguez, *Enhancing Photocatalytic Water Decontamination*, 2025, pp. 5–13.

32 R. Wahab, Y.-S. Kim, A. Mishra, S.-I. Yun and H.-S. Shin, *Nanoscale Res. Lett.*, 2010, **5**, 1675–1681.

33 B. J. Smug, M. Opalek, M. Necki and D. Wloch-Salamon, *Methods Ecol. Evol.*, 2024, **15**, 301–307.

34 Z. Breijyeh, B. Jubeh and R. Karaman, *Molecules*, 2020, **25**, 1340.

35 D. P. Linklater, V. A. Baulin, S. Juodkazis, R. J. Crawford, P. Stoodley and E. P. Ivanova, *Nat. Rev. Microbiol.*, 2021, **19**, 8–22.

36 W. R. Miller and C. A. Arias, *Nat. Rev. Microbiol.*, 2024, **22**, 598–616.

37 J. N. Pendleton, S. P. Gorman and B. F. Gilmore, *Expert Rev. Anti-infect. Ther.*, 2013, **11**, 297–308.

38 I. Ramdas and C. Devi, *J. Global Infect. Dis.*, 2020, **12**, 217.

39 M. M. Almoudi, A. S. Hussein, N. I. Mohd Sarmin and M. I. Abu Hassan, *Saudi Dent. J.*, 2023, **35**, 883–890.

40 M. Balouiri, M. Sadiki and S. K. Ibnsouda, *J. Pharm. Anal.*, 2016, **6**, 71–79.

41 H. Mikkelsen, Z. Duck, K. S. Lilley and M. Welch, *J. Bacteriol.*, 2007, **189**, 2411–2416.

42 J. Hasan, R. J. Crawford and E. P. Ivanova, *Trends Biotechnol.*, 2013, **31**, 295–304.

43 L. Z. Y. Huang, R. Penman, R. Kariuki, P. H. A. Vaillant, S. Gharehgozlo, Z. L. Shaw, V. K. Truong, J. Vongsvivut, A. Elbourne and R. A. Caruso, *Nanoscale*, 2025, **17**, 3170–3188.

44 S. Xu, T. Sun, Q. Xu, C. Duan, Y. Dai, L. Wang and Q. Song, *Nanoscale Res. Lett.*, 2018, **13**, 201.

45 Q. Tang, K. Wang, X. Ren, Q. Zhang, W. Lei, T. Jiang and D. Shi, *Sci. Total Environ.*, 2020, **715**, 137018.

46 V. Pitpisutkul and J. Prachayawarakorn, *Carbohydr. Polym.*, 2022, **298**, 120082.

47 A. Agrawal, N. Saini, K. Awasthi and A. Awasthi, *New J. Chem.*, 2024, **48**, 17013–17026.

48 X. Gao, Z. Yu, X. Tang, H. Zhang, L. Peng and J. Li, *J. Hazard. Mater.*, 2022, **436**, 129258.

49 R. E. Sjogren and M. J. Gibson, *Appl. Environ. Microbiol.*, 1981, **41**, 1331–1336.

50 K. Qi, B. Cheng, J. Yu and W. Ho, *J. Alloys Compd.*, 2017, **727**, 792–820.

51 J. Liu, Y. Wang, J. Ma, Y. Peng and A. Wang, *J. Alloys Compd.*, 2019, **783**, 898–918.

52 J. Hasan, R. J. Crawford and E. P. Ivanova, *Trends Biotechnol.*, 2013, **31**, 295–304.

53 A. Valiei, N. Lin, J.-F. Bryche, G. McKay, M. Canva, P. G. Charette, D. Nguyen, C. Moraes and N. Tufenkji, *Nano Lett.*, 2020, **20**, 5720–5727.

54 S. L. Arias, J. Devorkin, J. C. Spear, A. Civantos and J. P. Allain, *ACS Appl. Bio Mater.*, 2020, **3**, 7974–7988.

55 Z. Chen, Y. Gu, G. Wang, Q. Liu, Y. Li, Y. Weng, N. Lu, G. Yang and Y. Liu, *Langmuir*, 2022, **38**, 856–862.

56 N. Lin, A. Valiei, G. McKay, D. Nguyen, N. Tufenkji and C. Moraes, *ACS Biomater. Sci. Eng.*, 2022, **8**, 3122–3131.

57 A. Velic, A. Jaggessar, T. Tesfamichael, Z. Li and P. K. D. V. Yarlagadda, *Nanomaterials*, 2021, **11**, 2472.

58 N. Lin, P. Berton, C. Moraes, R. D. Rogers and N. Tufenkji, *Adv. Colloid Interface Sci.*, 2018, **252**, 55–68.

59 A. Roy and K. Chatterjee, *Nanoscale*, 2021, **13**, 647–658.

60 A. Hassanpour, M.-C. Groleau, D. Messaoudi, A. A. Greschner, K. Kohlmann, A. Ruediger, E. Déziel, S. Sun and M. A. Gauthier, *Mater. Adv.*, 2025, **6**, 4687–4695.

61 A. Hezam, Q. A. Drmosh, D. Ponnamma, M. A. Bajiri, M. Qamar, K. Namratha, M. Zare, M. B. Nayan, S. A. Onaizi and K. Byrappa, *Chem. Rec.*, 2022, **22**, 1–30.

62 J. Sen Chang, C. P. Saint, C. W. K. Chow, D. W. Bahnemann and M. N. Chong, *Int. Mater. Rev.*, 2024, **69**, 337–379.

63 I. Kim, K. Viswanathan, G. Kasi, S. Thanakkasaranee, K. Sadeghi and J. Seo, *Food Rev. Int.*, 2022, **38**, 537–565.

64 M. Zare, K. Namratha, S. Ilyas, A. Sultana, A. Hezam, S. L., M. A. Surmeneva, R. A. Surmenev, M. B. Nayan, S. Ramakrishna, S. Mathur and K. Byrappa, *ACS Food Sci. Technol.*, 2022, **2**, 763–781.

65 P. Makvandi, C. Wang, E. N. Zare, A. Borzacchiello, L. Niu and F. R. Tay, *Adv. Funct. Mater.*, 2020, **30**, 1910021.

66 X. Liu, D. P. Rodeheaver, J. C. White, A. M. Wright, L. M. Walker, F. Zhang and S. Shannon, *Regul. Toxicol. Pharmacol.*, 2018, **97**, 24–32.